

On anomalous optical beam shifts at near-normal incidence

Cite as: APL Photonics 7, 101301 (2022); <https://doi.org/10.1063/5.0111203>

Submitted: 18 July 2022 • Accepted: 27 September 2022 • Published Online: 28 October 2022

 M. Mazanov,  O. Yermakov,  A. Bogdanov, et al.



View Online



Export Citation



CrossMark

AMERICAN ELEMENTS
THE ADVANCED MATERIALS MANUFACTURER®

sapphire windows Nd:YAG
spintronics raman substrates
silver nanoparticles perovskites
MOCVD beta-barium borate
rare earth metals quantum dots
osmium scintillation Ce:YAG
refractory metals laser crystals
anode lithium niobate
dysprosium pellets MOFs
chalogenides
perovskite crystals

Nd:YAG yttrium iron garnet
zeolites III-V semiconductors
nano ribbons
epitaxial crystal growth
cerium oxide polishing powder
surface functionalized nanoparticles

Ca Sc Ti V Cr Mn Fe Co Ni Cu Zn Ga Ge As Se Br Kr
Sr Ba La Hf Ta W Re Os Ir Pt Au Hg Tl Pb Bi Po At Rn
Pb Ba La Hf Ta W Re Os Ir Pt Au Hg Tl Pb Bi Po At Rn
Ca Sr Ba La Hf Ta W Re Os Ir Pt Au Hg Tl Pb Bi Po At Rn
InAs wafers
AuNPs
CdTe
transparent ceramics

glassy carbon
III-V semiconductors
barium fluoride
ultra high purity materials
cerium oxide polishing powder
surface functionalized nanoparticles

beamsplitters
galium lump
europium phosphors
photons
transparent ceramics
cermet
nanodispersions
MBE grade materials
OLED lighting
sputtering targets
h-BN deposition slugs
CVD precursors

fused quartz
copper nanoparticles
infrared dyes
photronics
infrared dyes
thin film
solar energy
fiber optics
photovoltaics
borosilicate glass
superconductors
InGaAs
rutile
diamond micropowder
optical glass

additive manufacturing
organometallics
CIGS
cermet
nanodispersions
thin film
solar energy
fiber optics
photovoltaics
borosilicate glass
superconductors
InGaAs
rutile
diamond micropowder
optical glass

metamaterials
YBCO
indium tin oxide
MgF₂
rutile
diamond micropowder
optical glass

The Next Generation of Material Science Catalogs

Now Invent.™

www.americanelements.com

© 2021-2021. American Elements is a U.S. Registered Trademark.

On anomalous optical beam shifts at near-normal incidence

Cite as: APL Photon. 7, 101301 (2022); doi: 10.1063/5.0111203

Submitted: 18 July 2022 • Accepted: 27 September 2022 •

Published Online: 28 October 2022



View Online



Export Citation



CrossMark

M. Mazanov^{1,2} O. Yermakov,^{1,a)} A. Bogdanov,² and A. Lavrinenko³

AFFILIATIONS

¹V. N. Karazin Kharkiv National University, Kharkiv, Ukraine

²School of Physics and Engineering, ITMO University, St. Petersburg, Russia

³Department of Photonics Engineering, Technical University of Denmark, Kgs. Lyngby, Denmark

^{a)}Author to whom correspondence should be addressed: oe.yermakov@gmail.com

ABSTRACT

We develop the theory of optical beam shifts (both Goos–Hänchen and Imbert–Fedorov) for the case of near-normal incidence, when the incident angle becomes comparable with the angular beam divergence. The developed theory uncovers the unified origin of the anomalous beam shift enhancement via the geometric Berry phase singularity. Particularly, we predict the large Goos–Hänchen shift occurring for small incidence angles. We also propose a simple experimental scheme involving a quarter-wave q-plate that allows us to observe the giant transverse and longitudinal, spatial and angular beam shifts simultaneously. Finally, we analyze the relevant beam parameters, polarization structure, and intensity profiles of the shifted transmitted beam. Our results can find applications in spin–orbit photonics, polarization optics, sensing applications, and quantum weak measurements.

© 2022 Author(s). All article content, except where otherwise noted, is licensed under a Creative Commons Attribution (CC BY) license (<http://creativecommons.org/licenses/by/4.0/>). <https://doi.org/10.1063/5.0111203>

I. INTRODUCTION

The reflection and refraction of a plane electromagnetic wave at a dielectric interface are the basic physical processes inherent to all-optical systems and devices. They are rigorously described by the Snell's law and Fresnel equations. Nevertheless, in practice, we usually deal with optical beams for which the plane wave approximation is oversimplified. This results in the deviation from geometrical optics that manifests itself as spatial shifts of the beam known as the Goos–Hänchen (GH) and Imbert–Fedorov (IF) shifts. These shifts can be explained in terms of weak material-mediated interaction of the beam spectrum (*orbit state*) and its polarization (*spin state*).^{1–4}

Today, the GH and IF shifts, including the photonic spin Hall effect (PSHE) as a particular example of the IF shift, are well-studied in different systems including atomic optics, optical sensors, graphene, metasurfaces, polarizers, uniaxial crystals, etc.^{5–11} In general, the spatial (angular) beam shifts are very small—typically of the order of the light wavelength (the beam angular spectrum variance)—that limits their application.^{1–4} The shifts can be enhanced under several specific conditions including the near-Brewster incidence,^{12–15} material resonances,^{16,17}

exceptional points,¹⁸ and output beam polarization post-selection.¹⁹ In all these cases, the enhancement occurs at large angles of incidence (typically, tens of degrees). The standard theory of optical beam shifts⁴ fails to give an accurate explanation of shifts at near-normal incidence, while at the normal incidence they should completely disappear.

In this Letter, we develop a generalized theory of beam shifts covering the case of small incident angles comparable with the angular beam divergence. Usually, the longitudinal (GH) and transverse (IF) shifts are caused by different origins and considered independently.⁴ Here, we show that anomalously large GH and IF shifts have the same nature caused by the geometric Berry phase singularity and appeared simultaneously, for example, in phase plates and uniaxial slabs. While the partial cases of anomalous PSHE enhancement at near-normal incidence have been recently observed due to the spin-to-orbit angular momentum conversion,^{20–23} the GH shift is commonly known to exist only under total internal reflection conditions.⁴ Our theory predicts the giant GH shift at near-normal incidence and gives a simple practical guideline for the simultaneous experimental observation of the giant GH and IF shifts in a quarter-wave q-plate (QWQP).^{24–26}

II. EXTENDED THEORY OF OPTICAL BEAM SHIFTS

A. Standard theory of optical beam shifts

We consider first the oblique incidence of a monochromatic optical beam (under angle θ to the central plane wave of the beam) on a flat vacuum–medium interface; see Fig. 1.

The values of the shifts could be calculated within the Jones matrix formalism in the paraxial approximation. The Jones matrix \hat{T}^a relates the incident and reflected/transmitted plane wave amplitudes in the beam coordinate frame $|\mathbf{E}^a\rangle = \hat{T}^a(\theta, \mu, v)|\mathbf{E}\rangle$, where $|\mathbf{E}\rangle \propto |\mathbf{e}\rangle \cdot f(\mu, v)$ is the incident constituent plane-wave Jones vector, index $a = r, t$ denotes reflected and transmitted waves, respectively, $|\mathbf{e}\rangle = (e_x, e_y)^T$ is the Jones vector of the central plane wave in the incident beam, and $f(\mu, v)$ is the incident beam Fourier spectrum expressed in terms of the in-plane (μ) and out-of-plane (v) deflection angles of the non-central wave vectors.⁴

The linear ($\langle X^a \rangle, \langle Y^a \rangle$) and angular ($\langle P_X^a \rangle, \langle P_Y^a \rangle$) GH ($\langle X^a \rangle, \langle P_X^a \rangle$) and IF ($\langle Y^a \rangle, \langle P_Y^a \rangle$) shifts are then obtained using their original quantum-mechanical definition—the mean values of the coordinate and momentum operators calculated for the wavefunction of the beam,⁴

$$\begin{aligned} \langle X^a \rangle, \langle Y^a \rangle &= \langle \mathbf{E}^a | i\partial/\partial k_{X,Y}^a | \mathbf{E}^a \rangle / N^a, \\ \langle P_X^a \rangle, \langle P_Y^a \rangle &= \langle \mathbf{E}^a | k_{X,Y}^a | \mathbf{E}^a \rangle / N^a, \end{aligned} \quad (1)$$

where the integration is taken over the transverse momentum components $k_X^a = y^a k_0 \mu$ and $k_Y^a = k_0 v$ in the beam coordinate frame, $k_0 = 2\pi/\lambda$ is the light wavevector in vacuum, λ is the light wavelength, and factor $\{\gamma^{t,r}\} = \{1, -1\}$ accounts for the inversion of the x -components of the wavevectors with reflection. Here,

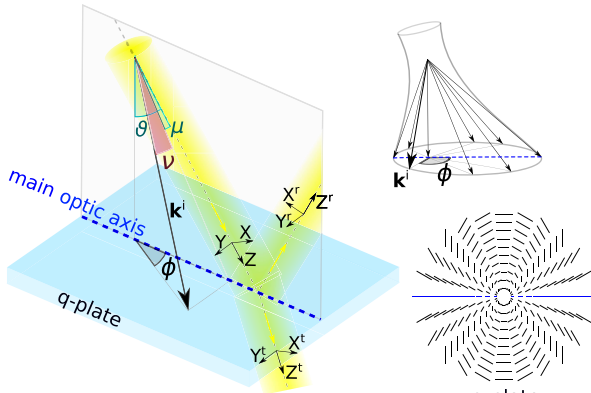


FIG. 1. Schematic geometry of the problem shows the reflection of the beam from the q-plate with $q = 2$. The long black arrow marks the non-central constituent plane wave with incident wavevector \mathbf{k}^i , angular in-plane (μ) and out-of-plane (v) deflection components. Its plane of incidence forms a polar deflection angle ϕ with a central plane wave (yellow arrows) incident under angle θ . The insets schematically show the incident wavevectors of the non-central plane waves of a beam forming the large polar deflection angles and the q-plate (in real or Fourier space) with the main optic axis marked by blue.

$N^a = \langle \mathbf{E}^a | \mathbf{E}^a \rangle$ is the normalization factor proportional to the beam intensity. At large incidence angles, the Jones matrix \hat{T}^a is a slowly varying function across the beam spectrum ($\partial \hat{T}^a / \partial k_{X,Y}^a \sim \lambda$), which leads to small shifts of the order of the light wavelength and angular beam spectrum variance for spatial and angular shifts, respectively (see the [supplementary material](#)).

B. Geometric Berry phase singularity

The standard theory⁴ predicts that at large incident angles θ , the deflection angle ϕ (see Fig. 1) is small and behaves as

$$\phi = \frac{v}{\sin \theta} \ll 1. \quad (2)$$

The obvious absence of an IF shift under the normal incidence on one hand and its singularity in approximate expressions for small incidence angles on another hand assume the sharp IF shift peak. To resolve this collision, we extend the standard theory analyzing the behavior of the deflection angle ϕ near the phase singularity occurring at normal incidence.

In this case, the deflection angles ϕ of the plane wave components, constituting the beam, cover a full 2π range, see the inset in Fig. 1. In a medium with spatial-dependent anisotropy, such as a q-plate (see the inset in Fig. 1), the wide spreading of the incidence planes results in the significant difference of Fresnel's amplitudes for different plane-wave components. Thus, under some specific conditions (anisotropy degree, optic axis orientation, the retardation phase of the anisotropic slab), the optical beam incident at sufficiently small angles can experience anomalously large beam shifts. To show this explicitly, we note that at near-normal incidence, Jones matrix $\hat{T}^a(\theta, \mu, v)$ depends on incident angle θ , in-plane μ and out-of-plane v deflections only implicitly, through the polar deflection angle ϕ [$\hat{T}^a(\theta, \mu, v) \equiv \hat{T}^a(\phi)$], where the latter could be approximated as follows (see the [supplementary material](#)),

$$\phi(\theta, \mu, v) \approx \tan^{-1} \left(\frac{v}{\theta + \mu} \right). \quad (3)$$

Equation (3) is the extension of the standard theory applicable for the near-normal incidence. When θ is of the order of beam divergence, one can notice from Eq. (3) that the polar deflection angle ϕ may be large enough for a finite portion of the beam spectrum, and even close to $\pm 90^\circ$ at $\theta \simeq -\mu$. Thus, Jones matrix $\hat{T}^a(\phi)$ is a rapidly changing function across the beam spectrum ($\partial \hat{T}^a / \partial k_{X,Y}^a \sim w_0 \gg \lambda$, where w_0 is the beam waist), which, in turn, will cause anomalous beam shifts (see Fig. S2 in the [supplementary material](#)).

In fact, the polar deflection angle at near-normal incidence ($\theta \rightarrow 0^\circ$) is equivalent to the geometric Berry phase, $\Phi_B = -\phi \cos \theta \simeq -\phi$.⁴ Thus, the considered geometric singularity of the polar deflection angle simultaneously means the Berry phase singularity. The large IF shift arises from large transverse momentum derivatives of the Berry phase across the beam spectrum according to its definition.

Another surprising consequence of Eq. (3) is that it leads to the anomalous GH shift. In conventional situation (large angles of incidence), the GH shifts are caused by the spatial dispersion of the scattering coefficients.⁴ In contrast, at near-normal incidence, GH shift arises from the large longitudinal momentum gradient of the

Berry phase across the lateral parts of the beam spectrum. Note that such longitudinal gradients caused by strong spin-orbit coupling are negligible at large incident angles. Thus, both GH and IF shifts under near-normal incidence are caused by the spatial gradient of the Berry phase and their giant enhancement at the specified angle of incidence is defined by the Berry phase singularity.

III. OPTICAL BEAM SHIFTS AT NEAR-NORMAL INCIDENCE

A. Derivation

To exhibit the near-normal Berry phase singularity as a particular example, we consider transmission through a q-plate with topological charge $q = 2$. Following the Jones matrix formalism in the k -space (see the [supplementary material](#) for the detailed derivation), we calculate analytically the GH and IF shifts of the Gaussian beam transmitted through the q-plate when the beam incidence plane is parallel to the waveplate main optic axis, which lies at the interface ([Fig. 1](#)). The Gaussian beam angular spectrum is defined by the Fourier spectrum $f(\mu, \nu) = \exp[-\kappa^2(\mu^2 + \nu^2)/2]$, where $\kappa = k_0 w_0 / \sqrt{2}$ is the inverse beam divergence. The case of q-plate in a real space is considered in the [supplementary material](#) by drawing an analogy between the near-normal and off-center beam incidence.

Using this approach, we show that any type of normalized beam shift under near-normal incidence $\langle \tilde{L} \rangle$ could be defined by the universal formula expressed as the multiplication of three factors: (i) geometric Berry phase singularity factor depending on the beam width and angle of incidence $G(\kappa\vartheta)$, (ii) polarization-related factor depending on the polarization (Stokes parameters) of the incident beam S , and (iii) material-related factor depending on Fresnel coefficients τ ,

$$\langle \tilde{L} \rangle = \sum_{i=1,2} G_i(\kappa\vartheta) \cdot S_i \cdot \tau_i. \quad (4)$$

Equation (4) allows us to distinguish the contributions and to evaluate the different cases. For instance, the near-normal geometric Berry phase singularity $G(\kappa\vartheta)$ could be suppressed by the material-related factor τ (see the [supplementary material](#), Sec. IV). Specific results for the four transmitted beam shifts read (see the [supplementary material](#) for the detailed derivation)

$$\langle \tilde{P}_X \rangle = \frac{\Lambda_X(\kappa\vartheta) \cdot S_1 \cdot \tau_-}{\vartheta N^t}, \quad (5)$$

$$\langle \tilde{P}_Y \rangle = \frac{\Lambda_Y(\kappa\vartheta) \cdot S_2 \cdot \tau_-}{\vartheta N^t}, \quad (6)$$

$$\langle \tilde{X} \rangle = -\gamma^t \frac{\Lambda_X(\kappa\vartheta) \cdot S_1 \cdot \tau_\times}{\vartheta N^t}, \quad (7)$$

$$\langle \tilde{Y} \rangle = -\frac{\Lambda_Y(\kappa\vartheta) \cdot S_2 \cdot \tau_\times}{\vartheta N^t} - \frac{\Lambda_{SHE}(\kappa\vartheta) \cdot S_3 \cdot |t_-|^2}{\vartheta N^t}, \quad (8)$$

where $S_1 = |e_x|^2 - |e_y|^2$, $S_2 = 2\Re[e_x^* e_y]$, and $S_3 = 2\Im[e_x^* e_y]$ are the corresponding Stokes parameters of the incident beam,

$N^t = [\tau_+ + \tau_- S_1 \Lambda_Y(\kappa\vartheta)]/2$ is the squared norm of the transmitted beam, $t_- = t_e - t_o$, $\tau_{+-} = |t_e|^2 \pm |t_o|^2$, and $\tau_\times = 2\Im(t_e t_o^*)$ are real coefficients depending on the ordinary t_o and extraordinary t_e transmission amplitudes for the plane wave under normal incidence (see the [supplementary material](#)). Hereinafter, we use the dimensionless shift values defined as $\langle \tilde{P}_{X,Y} \rangle = \langle P_{X,Y} \rangle \cdot \kappa^2/k$ and $\langle \tilde{X}, \tilde{Y} \rangle = \langle X, Y \rangle \cdot k$. The nonlinear geometric resonant factors Λ_X , Λ_Y , and Λ_{SHE} are the following:

$$\begin{aligned} \Lambda_X(\kappa\vartheta) &= \frac{(6 + 4\kappa^2\vartheta^2 + \kappa^4\vartheta^4)e^{-\kappa^2\vartheta^2} + 2\kappa^2\vartheta^2 - 6}{\kappa^4\vartheta^4}, \\ \Lambda_Y(\kappa\vartheta) &= \frac{6 - 4\kappa^2\vartheta^2 + \kappa^4\vartheta^4 - 2e^{-\kappa^2\vartheta^2}(\kappa^2\vartheta^2 + 3)}{\kappa^4\vartheta^4}, \\ \Lambda_{SHE}(\kappa\vartheta) &= 1 - e^{-\kappa^2\vartheta^2}. \end{aligned} \quad (9)$$

Note that the squared norm of transmitted beam state $N^t(\vartheta)$ plays a role of a slight renormalization, in sharp contrast to large incident angles cases, where it causes singularity in the shifts by approaching zero.^{12–19,27} For the reflected beam, we arrive at the same results as in Eqs. (5)–(8) with substitutions $\{t_e, t_o\} \rightarrow \{r_e, r_o\}$, $\gamma^t \rightarrow \gamma^r$, and $N^t \rightarrow N^r$. For the q-plates with other nonzero q , the shifts are similar to Eqs. (5)–(8), but with different nonlinear functions (9).

B. Analysis

Equations (4)–(8) are the main results of this work applicable for any cases except $\kappa\vartheta \gg 1$. They describe both GH and IF shifts at near-normal incidence for the arbitrary anisotropic slab, q-plate or metasurface. One can see that each shift in Eqs. (5)–(8) is the product of three factors in a good agreement with Eq. (4). The second term in expression (8) for the spatial IF shift is a counterpart of the anomalous PSHE connected with the circular polarization of the incident beam. Moreover, due to the presence of the first term in Eq. (8), the IF shift can be obtained with the arbitrary polarization state except pure TM- and TE-polarization, i.e., along ($S_1 = 1$) and across ($S_1 = -1$) the main optic axis.

We also note the remarkable connection of the four shifts to the geometric resonant terms $\Lambda_{X,Y}$. First, there is a proportionality between the spatial and angular shifts, which is only broken by the spin-Hall term in Eq. (8). The simultaneous appearance of the spatial and angular GH and IF shifts at the same angle of incidence is unique. At large incident angles ($\kappa\vartheta \gg 1$), the GH shifts can be simultaneously observed only in special cases such as lossy media²⁸ or vortex beams.²⁹ Second, there is a further similarity of geometric resonant terms along Y and X directions, whereas $\Lambda_X(\kappa\vartheta) = e^{-\kappa^2\vartheta^2} \Lambda_Y(i\kappa\vartheta)$. This reflects the fact that all anomalous near-normal incident shifts have the same origin, namely, the geometric Berry phase singularity. As a consequence, all four types of anomalously large optical beam shifts (GH and IF, linear and angular) could be detected simultaneously in the near-normal incidence regime ($\kappa\vartheta \lesssim 1$), particularly in the vicinity of $\vartheta = 0.2^\circ$ using the proposed material platform, beam parameters, and elliptical polarization of incident light. The detection of shifts could be further enhanced with even higher precision by using the weak measurements technique in the darkfield region.³⁰

Figure 2 shows the optical beam shift dependencies on the incidence angle for the beam transmitted through the QWQP with

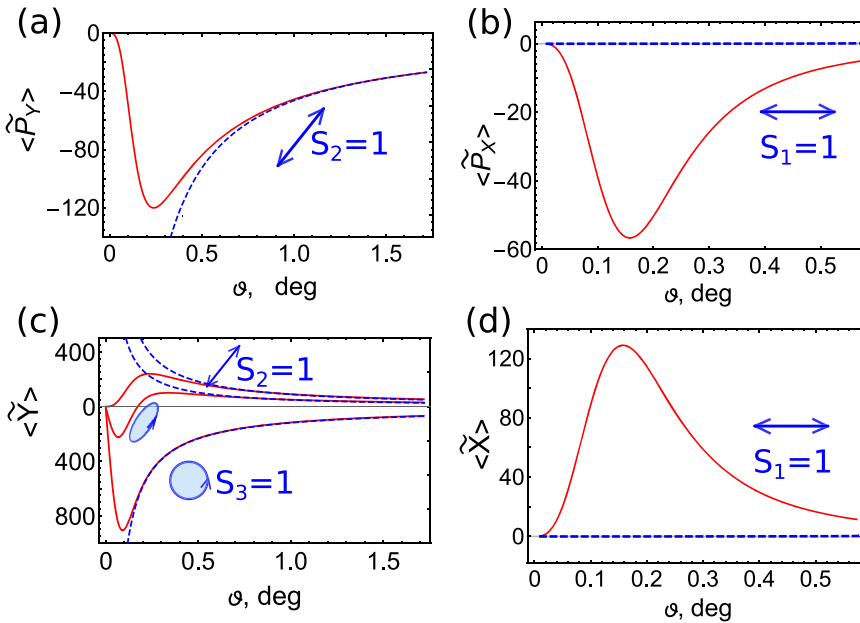


FIG. 2. Resonant angular IF (a), angular GH (b), spatial IF (c), and spatial GH (d) shifts of the beam incident near-normally at a QWQP [curve with one node in panel (c) corresponds to elliptic input polarization with Stokes parameters $S_2 = 0.95, S_3 = 0.31$]. The blue dashed lines correspond to the standard theory ($\kappa\theta \gg 1$), so that for IF shifts, Eq. (2) holds, while GH shifts are zero (see the [supplementary material](#)). Parameters: $q = 2, n_0 = 2.6, n_e = 2.7, d_z = 7.5\lambda$ ($\tau_- = -0.58, \tau_x = -1.32, |\tau_-|^2 = 1.44$, and $\tau_+ = 1.42$).

$q = 2$ and the main optic axis lying in the beam plane of incidence. It is important to note that a linear IF shift can change the shift direction to the opposite one at some angle under elliptically-polarized beam illumination [Fig. 2(c)]. This is caused by the interplay between differently polarized terms of the linear IF shift [Eq. (8)]. The developed theory [Eq. (8)] also describes the switching of the IF direction for strongly anisotropic systems due to the polarization mixing, especially when the optical axis is arbitrarily oriented.³¹

C. Impact of beam width and slab material

The optical beam shifts under near-normal incidence depend substantially on the beam waist w_0 via the inverse beam divergence κ , as it is expressed by nonlinear functions $\Lambda_{X,Y}(\kappa\theta)$ [Eq. (9)]. The IF shifts are anomalous and have asymptotes $\propto 1/\theta$ at large incidence angles ($\kappa\theta \gg 1$), which is hinted by the standard theory.⁴ The GH shifts have higher-order asymptotes at large incident angles $\propto 1/(\theta^3\kappa^2)$ (Fig. 3). This explains why the anomaly in GH shifts was not anticipated by the standard theory, in which the spatial GH shift is absent except the case of total internal reflection. Moreover, one can notice that the amplitude of the optical beam shift peak is proportional to the beam waist w_0 , while the corresponding critical angle is inversely proportional to it (see the inset in Fig. 3). In general, the critical angle corresponding to the maxima of GH and IF shifts is about a few tenths of a degree for a beam width of several dozen microns at $\lambda = 630$ nm. This result completely agrees with the recent experimental observations of the anomalous PSHE under near-normal incidence at hyperbolic metamaterials and anisotropic slabs.^{20–23} Finally, we highlight the connection between the Berry phase singularity and optical beam shifts. The resonant angles of $G_X(\kappa\theta)$ and $G_Y(\kappa\theta)$ in Fig. 3 (about 0.15° and 0.25° for $\kappa = 700$, respectively) fit well with the giant peaks in angular dependences of all four types of beam shifts shown in Fig. 2. However, for linear

IF shift, the peaks may be slightly shifted within the range $0.1^\circ < \theta < 0.3^\circ$ due to the non-trivial polarization dependence [Eq. (8)].

All material dependencies in Eqs. (5)–(8) are factored out in four dimensionless coefficients, τ_+, τ_-, τ_x , and t_- . We analyzed the maximum values of these parameters as functions of the retardation and average refractive index of the waveplate (see the [supplementary material](#)), and concluded that the low-birefringent

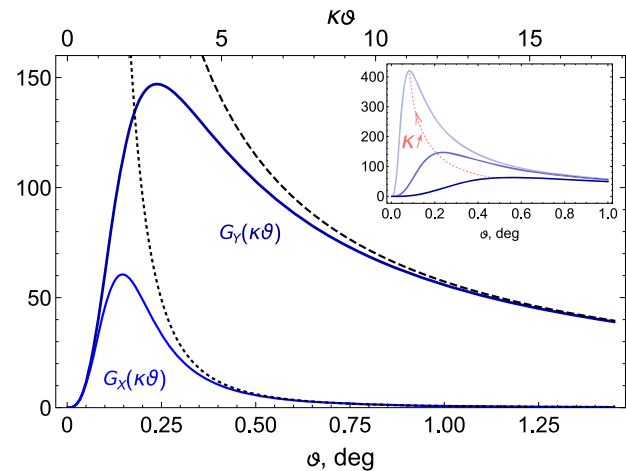


FIG. 3. Nonlinear geometric Berry phase singularity terms (9) appearing in shifts (5)–(8): $G_Y(\kappa\theta) = \Lambda_Y(\kappa\theta)/\theta$ (dark blue) and $G_X(\kappa\theta) = \Lambda_X(\kappa\theta)/\theta$ (light blue), along with their asymptotes at large incidence angles $1/\theta$ (dashed black) and $2/(\kappa^2\theta^3)$ (dotted black), respectively. Here, we used the inverse beam divergence $\kappa = 700$, namely, $\lambda = 630$ nm, $w_0 \approx 100 \mu\text{m}$. The inset shows the dependence of $G_Y(\kappa\theta)$ on the inverse beam divergence κ . The arrow indicates the sequence of increasing beam waist, $\kappa = 300, 700, 2000$, respectively.

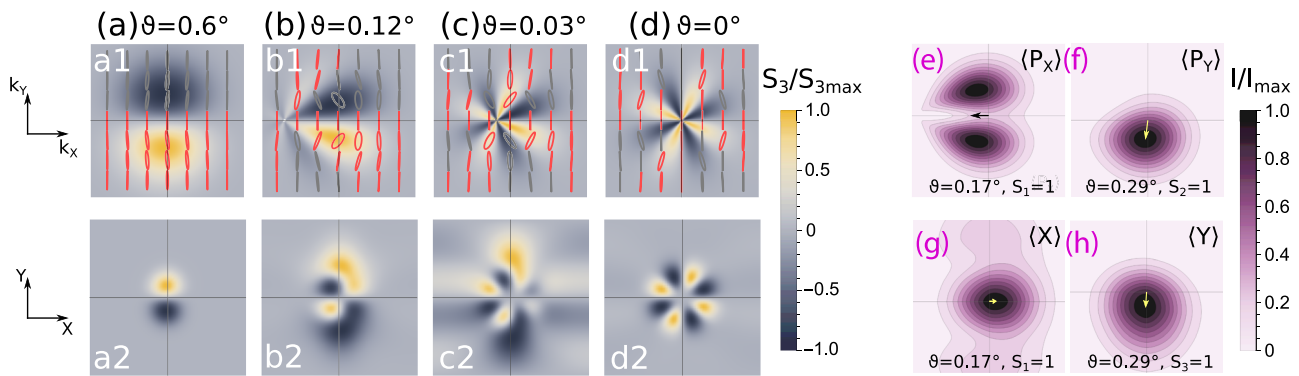


FIG. 4. Panels (a)–(d): normalized helicity (Stokes parameter S_3) patterns in k -space (a1)–(d1) and in real space (a2)–(d2) in the transmitted beam coordinate frame for the ordinary polarized ($S_1 = 1$) beam near-normally transmitted through QWQP. The ellipses in panels (a1)–(d1) indicate the corresponding polarization profile in k -space. Panels (e)–(h): intensity profiles at maximum linear and angular GH and IF shifts of the intensity centroid (shown by arrows) of the transmitted beam for their respective eigenpolarizations. Parameters are the same as in Fig. 2. The plots in the panels are the squares with the side $10w_0$ for all real-space panels, and $10/\kappa$ for all k -space panels.

QWQP is a perfect candidate for observing all four types of anomalous shifts simultaneously (although PSHE has a maximum for a half-wave q-plate).

D. Intensity and helicity profiles of anomalously shifted beam

To gain deeper insight into the physics of the anomalous beam shifts, we analyze the intensity and helicity (S_3) patterns for the transmitted TM-polarized beam ($S_1 = 1$) with Jones matrix \hat{T}^t (Fig. 4). When the incidence angle θ exceeds the beam divergence $1/\kappa$, PSHE naturally occurs owing to the so-called circular birefringence [Fig. 4(a)].⁷ At near-normal incidence $\theta \lesssim 1/\kappa$, the spin-Hall doublets from lateral and opposite parts of the beam Fourier spectrum become prominent, and an octupole helicity profile is built up in k -space with a phase singularity at a distance $\sim k_0 \theta$ from the geometric-optics beam axis [Figs. 4(b) and 4(c)]. In real space, at $\theta = 0^\circ$, the helicity is carried by a mode resembling a Bessel-Gaussian mode with $m = 4^{32}$ and null intensity on the beam axis [Fig. 4(d)]. The anomalously large shift and the presence of polarization singularity provide a close connection to the superoscillations.³³ Finally, we demonstrate explicitly the beam shifts of all four kinds in Figs. 4(e)–4(h). The anomalous GH angular shifts are accompanied by noticeable transverse beam spectrum deformations around the polarization singularity [Fig. 4(e)].

IV. CONCLUSION

To conclude, we have developed a generalized theory of spatial and angular beam shifts applicable to the case of the near-normal incidence, when the angle of incidence becomes comparable with the beam divergence. The principal point of the theory is that anomalously large shifts of all types are shown to have the same fundamental origin—the singularity in the Berry phase appearing in the beam Fourier spectrum. The theory also predicts the anomalous GH shifts at the near-normal incidence. The results have been illustrated for an analytically treated example of a quarter-wave

q-plate with $q = 2$ supporting anomalously large simultaneous near-normal incidence shifts of all kinds in manifold times exceeding shifts observed separately in conventional cases. Thus, the anomalous near-normal shifts are completely feasible for direct experimental verification.

The predicted effects could arise for other types of waves (acoustic, electron beams, etc.), physical platforms (bound states in the continuum,³⁴ q-^{24,25} and j-plates^{35,36}) and material-anisotropy types (biaxial and bianisotropic media). Finally, we conduct the analogy between the beam shifts under near-normal incidence and the near-field spin Hall effect^{37–39} manifested as the high-directional polarization-dependent surface wave excitation by means of a dielectric antenna.^{40,41} In this case, the role of inverse beam divergence may be played by the ratio of antenna's characteristic size to the incident wavelength.

SUPPLEMENTARY MATERIAL

The [supplementary material](#) contains five sections. Section I provides the detailed discussion on the polar deflection angle and the geometric Berry phase singularity at near-normal incidence. Section II goes through the derivation of the Jones matrix under near-normal incidence for the q-plate. Section III gives the analysis of the impact of the material platform on the optical beam shifts. Section IV covers the case of the isotropic slab and gives the detailed calculations of near-normal optical beam shifts. Sections V and VI go through the detailed derivation of near-normal-incidence shifts for a q-plate in Fourier and real spaces, respectively.

ACKNOWLEDGMENTS

O.Y. acknowledges support from the Ministry of Education and Science of Ukraine under Grant No. 0122U001482. A.B. acknowledges the BASIS foundation, the Ministry of Science and Higher Education of the Russian Federation (No. 075-15-2022-1120), and the academic leadership program Priority 2030.

AUTHOR DECLARATIONS**Conflict of Interest**

The authors have no conflicts to disclose.

Author Contributions

M. Mazanov: Formal analysis (equal); Investigation (equal); Methodology (equal); Software (lead); Validation (equal); Visualization (equal); Writing – original draft (equal); Writing – review & editing (equal). **O. Yermakov:** Conceptualization (equal); Formal analysis (equal); Investigation (equal); Methodology (equal); Supervision (equal); Validation (equal); Visualization (equal); Writing – original draft (lead); Writing – review & editing (equal). **A. Bogdanov:** Conceptualization (equal); Investigation (equal); Supervision (equal); Validation (equal); Writing – review & editing (equal). **A. Lavrinenko:** Conceptualization (equal); Investigation (equal); Methodology (equal); Supervision (equal); Validation (equal); Writing – review & editing (equal).

DATA AVAILABILITY

The data that support the findings of this study are available within the article and its [supplementary material](#).

REFERENCES

- ¹M. R. Dennis and J. B. Götte, “The analogy between optical beam shifts and quantum weak measurements,” *New J. Phys.* **14**, 073013 (2012).
- ²J. B. Götte and M. R. Dennis, “Generalized shifts and weak values for polarization components of reflected light beams,” *New J. Phys.* **14**, 073016 (2012).
- ³F. Töppel, M. Ornigotti, and A. Aiello, “Goos–Hänchen and Imbert–Fedorov shifts from a quantum-mechanical perspective,” *New J. Phys.* **15**, 113059 (2013).
- ⁴K. Y. Bliokh and A. Aiello, “Goos–Hänchen and Imbert–Fedorov beam shifts: An overview,” *J. Opt.* **15**, 014001 (2013).
- ⁵C. Menzel, C. Rockstuhl, T. Paul, S. Fahr, and F. Lederer, “Imbert–Fedorov shift at metamaterial interfaces,” *Phys. Rev. A* **77**, 013810 (2008).
- ⁶X. Yin, Z. Ye, J. Rho, Y. Wang, and X. Zhang, “Photonic spin Hall effect at metasurfaces,” *Science* **339**, 1405–1407 (2013).
- ⁷K. Y. Bliokh, C. T. Samsan, C. Prajapati, G. Puentes, N. K. Viswanathan, and F. Nori, “Spin-Hall effect and circular birefringence of a uniaxial crystal plate,” *Optica* **3**, 1039–1047 (2016).
- ⁸X. Ling, X. Zhou, K. Huang, Y. Liu, C.-W. Qiu, H. Luo, and S. Wen, “Recent advances in the spin Hall effect of light,” *Rep. Prog. Phys.* **80**, 066401 (2017).
- ⁹K. Y. Bliokh, C. Prajapati, C. T. Samsan, N. K. Viswanathan, and F. Nori, “Spin-Hall effect of light at a tilted polarizer,” *Opt. Lett.* **44**, 4781–4784 (2019).
- ¹⁰H. Li, C. Ma, J. Wang, M. Tang, and X. Li, “Spin-orbit Hall effect in the tight focusing of a radially polarized vortex beam,” *Opt. Express* **29**, 39419–39427 (2021).
- ¹¹S. N. Khonina and I. Golub, “Vectorial spin Hall effect of light upon tight focusing,” *Opt. Lett.* **47**, 2166–2169 (2022).
- ¹²J. B. Götte, W. Löfller, and M. R. Dennis, “Eigenpolarizations for giant transverse optical beam shifts,” *Phys. Rev. Lett.* **112**, 233901 (2014).
- ¹³J. B. Götte and M. R. Dennis, “Limits to superweak amplification of beam shifts,” *Opt. Lett.* **38**, 2295–2297 (2013).
- ¹⁴A. Aiello, M. Merano, and J. P. Woerdman, “Brewster cross polarization,” *Opt. Lett.* **34**, 1207–1209 (2009).
- ¹⁵M. Merano, A. Aiello, M. P. Van Exter, and J. P. Woerdman, “Observing angular deviations in the specular reflection of a light beam,” *Nat. Photonics* **3**, 337–340 (2009).
- ¹⁶I. V. Soboleva, V. V. Moskalenko, and A. A. Fedyanin, “Giant Goos–Hänchen effect and Fano resonance at photonic crystal surfaces,” *Phys. Rev. Lett.* **108**, 123901 (2012).
- ¹⁷L. Salasnich, “Enhancement of four reflection shifts by a three-layer surface-plasmon resonance,” *Phys. Rev. A* **86**, 055801 (2012).
- ¹⁸X. Zhou, X. Lin, Z. Xiao, T. Low, A. Alù, B. Zhang, and H. Sun, “Controlling photonic spin Hall effect via exceptional points,” *Phys. Rev. B* **100**, 115429 (2019).
- ¹⁹O. Hosten and P. Kwiat, “Observation of the spin Hall effect of light via weak measurements,” *Science* **319**, 787–790 (2008).
- ²⁰O. Takayama, J. Sukham, R. Malureanu, A. V. Lavrinenko, and G. Puentes, “Photonic spin Hall effect in hyperbolic metamaterials at visible wavelengths,” *Opt. Lett.* **43**, 4602–4605 (2018).
- ²¹M. Kim, D. Lee, T. H. Kim, Y. Yang, H. J. Park, and J. Rho, “Observation of enhanced optical spin Hall effect in a vertical hyperbolic metamaterial,” *ACS Photonics* **6**, 2530–2536 (2019).
- ²²W. Zhu, H. Zheng, Y. Zhong, J. Yu, and Z. Chen, “Wave-vector-varying Pancharatnam-Berry phase photonic spin Hall effect,” *Phys. Rev. Lett.* **126**, 083901 (2021).
- ²³X. Ling, F. Guan, X. Cai, S. Ma, H.-X. Xu, Q. He, S. Xiao, and L. Zhou, “Topology-induced phase transitions in spin-orbit photonics,” *Laser Photonics Rev.* **15**, 2000492 (2021).
- ²⁴L. Marrucci, C. Manzo, and D. Paparo, “Optical spin-to-orbital angular momentum conversion in inhomogeneous anisotropic media,” *Phys. Rev. Lett.* **96**, 163905 (2006).
- ²⁵L. Marrucci, E. Karimi, S. Slussarenko, B. Piccirillo, E. Santamato, E. Nagali, and F. Sciarrino, “Spin-to-orbital conversion of the angular momentum of light and its classical and quantum applications,” *J. Opt.* **13**, 064001 (2011).
- ²⁶H. Larocque, J. Gagnon-Bischoff, F. Bouchard, R. Fickler, J. Upham, R. W. Boyd, and E. Karimi, “Arbitrary optical wavefront shaping via spin-to-orbit coupling,” *J. Opt.* **18**, 124002 (2016).
- ²⁷Y. Gorodetski, K. Y. Bliokh, B. Stein, C. Genet, N. Shitrit, V. Kleiner, E. Hasman, and T. W. Ebbesen, “Weak measurements of light chirality with a plasmonic slit,” *Phys. Rev. Lett.* **109**, 013901 (2012).
- ²⁸A. Aiello, M. Merano, and J. P. Woerdman, “Duality between spatial and angular shift in optical reflection,” *Phys. Rev. A* **80**, 061801 (2009).
- ²⁹K. Y. Bliokh, I. V. Shadrivov, and Y. S. Kivshar, “Goos–Hänchen and Imbert–Fedorov shifts of polarized vortex beams,” *Opt. Lett.* **34**, 389–391 (2009).
- ³⁰U. Baishya, N. Kumar, and N. K. Viswanathan, “Dark-field spin Hall effect of light,” *Opt. Lett.* **47**, 4479–4482 (2022).
- ³¹M. Mazanov, O. Yermakov, I. Deriy, O. Takayama, A. Bogdanov, and A. V. Lavrinenko, “Photonic spin Hall effect: Contribution of polarization mixing caused by anisotropy,” *Quantum Rep.* **2**, 489–500 (2020).
- ³²A. Ito, Y. Kozawa, and S. Sato, “Generation of hollow scalar and vector beams using a spot-defect mirror,” *J. Opt. Soc. Am. A* **27**, 2072–2077 (2010).
- ³³M. Berry, N. Zheludev, Y. Aharonov, F. Colombo, I. Sabadini, D. C. Struppa, J. Tollakson, E. T. F. Rogers, F. Qin, M. Hong, X. Luo, R. Remez, A. Arie, J. B. Götte, M. R. Dennis, A. M. H. Wong, G. V. Eleftheriades, Y. Eliezer, A. Bahabad, G. Chen, Z. Wen, G. Liang, C. Hao, C.-W. Qiu, A. Kempf, E. Katzav, and M. Schwartz, “Roadmap on superoscillations,” *J. Opt.* **21**, 053002 (2019).
- ³⁴B. Wang, W. Liu, M. Zhao, J. Wang, Y. Zhang, A. Chen, F. Guan, X. Liu, L. Shi, and J. Zi, “Generating optical vortex beams by momentum-space polarization vortices centred at bound states in the continuum,” *Nat. Photonics* **14**, 623–628 (2020).
- ³⁵J. P. Balthasar Mueller, N. A. Rubin, R. C. Devlin, B. Groever, and F. Capasso, “Metasurface polarization optics: Independent phase control of arbitrary orthogonal states of polarization,” *Phys. Rev. Lett.* **118**, 113901 (2017).
- ³⁶R. C. Devlin, A. Ambrosio, N. A. Rubin, J. P. B. Mueller, and F. Capasso, “Arbitrary spin-to-orbital angular momentum conversion of light,” *Science* **358**, 896–901 (2017).
- ³⁷F. J. Rodríguez-Fortuño, G. Marino, P. Ginzburg, D. O’Connor, A. Martínez, G. A. Wurtz, and A. V. Zayats, “Near-field interference for the unidirectional excitation of electromagnetic guided modes,” *Science* **340**, 328–330 (2013).
- ³⁸P. V. Kapitanova, P. Ginzburg, F. J. Rodríguez-Fortuño, D. S. Filonov, P. M. Voroshilov, P. A. Belov, A. N. Poddubny, Y. S. Kivshar, G. A. Wurtz, and A. V. Zayats, “Photonic spin Hall effect in hyperbolic metamaterials for polarization-controlled routing of subwavelength modes,” *Nat. Commun.* **5**, 3226 (2014).

³⁹D. O'Connor, P. Ginzburg, F. J. Rodríguez-Fortuño, G. A. Wurtz, and A. V. Zayats, "Spin-orbit coupling in surface plasmon scattering by nanostructures," *Nat. Commun.* **5**, 5327 (2014).

⁴⁰I. S. Sinev, A. A. Bogdanov, F. E. Komissarenko, K. S. Frizyuk, M. I. Petrov, I. S. Mukhin, S. V. Makarov, A. K. Samusev, A. V. Lavrinenko, and I. V. Iorsh,

"Chirality driven by magnetic dipole response for demultiplexing of surface waves," *Laser Photonics Rev.* **11**, 1700168 (2017).

⁴¹I. Sinev, F. Komissarenko, I. Iorsh, D. Permyakov, A. Samusev, and A. Bogdanov, "Steering of guided light with dielectric nanoantennas," *ACS Photonics* **7**, 680–686 (2020).